

# Population transfer and rapid passage effects in a low pressure gas using a continuous wave quantum cascade laser

E. A. McCormack,<sup>1</sup> H. S. Lowth,<sup>1</sup> M. T. Bell,<sup>1</sup> D. Weidmann,<sup>1,2</sup> and G. A. D. Ritchie<sup>1,a)</sup>

<sup>1</sup>*Department of Chemistry, The Physical and Theoretical Chemistry Laboratory, The University of Oxford, South Parks Road, Oxford OX1 3QZ, United Kingdom*

<sup>2</sup>*Space Science and Technology Department, STFC Rutherford Appleton Laboratory, Harwell Oxford Campus, Didcot OX11 0QX, United Kingdom*

(Received 10 May 2012; accepted 18 June 2012; published online 17 July 2012)

A continuous wave quantum cascade laser (cw-QCL) operating at 10  $\mu\text{m}$  has been used to record absorption spectra of low pressure samples of OCS in an astigmatic Herriott cell. As a result of the frequency chirp of the laser, the spectra show clearly the effects of rapid passage on the absorption line shape. At the low chirp rates that can be obtained with the cw-QCL, population transfer between rovibrational quantum states is predicted to be much more efficient than in typical pulsed QCL experiments. This optical pumping is investigated by solving the Maxwell Bloch equations to simulate the propagation of the laser radiation through an inhomogeneously broadened two-level system. The calculated absorption profiles show good quantitative agreement with those measured experimentally over a range of chirp rates and optical thicknesses. It is predicted that at a low chirp rate of 0.13 MHz ns<sup>-1</sup>, the population transfer between rovibrational quantum states is 12%, considerably more than that obtained at the higher chirp rates utilised in pulsed QCL experiments. © 2012 American Institute of Physics. [<http://dx.doi.org/10.1063/1.4734020>]

## I. INTRODUCTION

Continuous wave quantum cascade laser (QCL) devices are high resolution and intense sources of single mode radiation.<sup>1-3</sup> These properties make QCLs ideal for use in nonlinear spectroscopy experiments, such as Lamb-dip,<sup>4</sup> free induction decay,<sup>5,6</sup> and rapid passage studies. In addition to these types of spectroscopic applications, QCLs may also be used to prepare molecules in specific rovibrational quantum states. This approach to quantum state preparation has been demonstrated recently using two cw-QCLs in a pump-probe type arrangement.<sup>7</sup> In Ref. 7, a high-powered, narrow linewidth (2 MHz) pump cw-QCL was used at a low chirp rate (0.1 MHz ns<sup>-1</sup>), and it was shown that ~16% of the  $v = 0, J = 6.5, \Omega = \frac{1}{2}$  level of NO was transferred to the  $v = 1$  level. This population transfer was calculated from the saturation parameters of the system under the experimental conditions,<sup>8</sup> and was consistent with the value predicted by solving the Maxwell Bloch equations for these levels. While a 16% transfer of population is not particularly high, it does, however, indicate the potential use of cw-QCLs for rovibrational state preparation of molecules for experiments in reaction dynamics and kinetics, thereby allowing the internal state dependence of energy transfer and chemical reactivity to be probed.<sup>9-12</sup> In this paper we extend the study of Walker *et al.*,<sup>7</sup> and discuss rapid passage signals and population transfer effects occurring when a cw-QCL is operated at chirp rates in the range ~0.1–1 MHz ns<sup>-1</sup> in a single laser arrangement, considerably lower than the 10–200 MHz ns<sup>-1</sup> typically obtained with pulsed QCL systems.

The degree of population transfer between two molecular states that can be achieved in a typical experiment using chirped laser radiation depends on the rate at which the laser frequency is swept through the molecular resonance. The sweep through the transition is typically described as being either linear or adiabatic, depending on whether the square of the on-resonance Rabi frequency is approximately equal to, or much greater than, the laser chirp rate, respectively.<sup>13</sup> The adiabatic passage regime is favourable for state preparation experiments as the extent of population transfer is relatively insensitive to drifts in laser frequency, intensity, and pulse lengths, in comparison to, e.g., a single  $\pi$ -pulse of resonant radiation. Development of the adiabatic approach was first carried out for magnetic resonance experiments, using a slowly varying magnetic field to drive transitions between nuclear spin states.<sup>14</sup> Subsequently, adiabatic passage has been used for coherent population transfer in many fields (see Ref. 15), using atomic electronic transitions,<sup>16</sup> and, to a lesser degree, in the infrared region (using, e.g., a cw-N<sub>2</sub>O laser).<sup>17-19</sup>

The conditions for adiabatic transfer to occur require<sup>13</sup> that  $\Omega_0^2 \gg |d\Delta/dt|$ , where  $\Omega_0 = d \times \mathcal{E}/\hbar$  is the on-resonance Rabi frequency,  $d$  is the transition dipole moment,  $\mathcal{E}$  is the electric field strength of the radiation, and  $\hbar$  is the reduced Planck's constant. The detuning is defined as  $\Delta(t) = \omega_0 - \omega(t)$ , where  $\omega_0$  is the resonance transition frequency, and  $\omega(t)$  is the radiation frequency. Therefore, if the Rabi frequency is high, and the time taken to sweep through a resonance is long, then population transfer can be 100% under the adiabatic regime.<sup>20</sup> This analysis assumes that relaxation processes are negligible in the time that the frequency sweeps through the transition, so that coherence is maintained. In this case, because the population transfer has occurred in a time

<sup>a)</sup>Electronic mail: grant.ritchie@chem.ox.ac.uk.

shorter than the radiative or collisional lifetime of the excited state, it is named rapid adiabatic passage.

To date, most QCL studies have employed pulsed QCL devices,<sup>21</sup> in which the power of the laser increases rapidly from zero through rapid heating of the laser chip within a single electrical pulse of tens to hundreds of nanoseconds duration. This Joule heating leads to a fast frequency chirp of the laser output over a wavenumber range that is large ( $\sim 1\text{--}2\text{ cm}^{-1}$ ) compared to a typical molecular resonance.<sup>22</sup> The fast sweep rate of the laser radiation through a molecular transition results in an asymmetric absorption line shape, often exhibiting post-resonance oscillations (if measured with a fast detector). As the laser radiation is swept rapidly through the molecular resonance, an oscillating polarisation density is produced in the sample, along with population of the upper molecular state. While the laser frequency remains close to resonance, the induced polarisation interferes destructively with the laser electric field, resulting in attenuation of the propagating radiation. However, as the laser frequency moves away from the resonance, beating occurs between the polarised sample and laser field. For this beating to be observable, the time scale for relaxation of the induced polarisation must be sufficiently long in comparison with the time taken for the laser frequency to traverse the resonance. Consequently, these so-called ‘‘rapid passage effects’’ are most pronounced in absorption spectra measured in low pressure samples using rapidly swept radiation. A conventional absorption line shape can be recovered by the addition of a non-absorbing gas to decrease the relaxation time of the system.<sup>23,24</sup>

The population transfer for most pulsed QCL experiments is minimal, due to the fast chirp rate (tens to hundreds of MHz ns<sup>-1</sup>), and so the system is likely to be operated in the linear passage regime (as  $\Omega_0^2$  will be smaller than the chirp rate, e.g., in the experiments in this paper  $\Omega_0 = 3$  MHz), which is of limited use in population transfer experiments. By using cw-QCLs, much lower chirp rates can be achieved in comparison to pulsed QCL systems as the cw-QCL laser chip can dissipate heat more effectively, so that the initial power is higher and a smaller modulation of the driving current is applied. Therefore, a low chirp rate can be achieved (tens to hundreds of kHz ns<sup>-1</sup>), so that the adiabatic regime may be reached and a larger population transfer may occur. To this end, the effect of low chirp rates on the degree of population transfer from the  $2\nu_2$  P(42) state of OCS at  $10\text{ }\mu\text{m}$  is investigated in this paper.

To better understand the observed absorption spectra under a rapid passage (RP) regime, and quantify the population transfer achieved, the coupled Maxwell Bloch equations describing the propagation of the laser radiation through the absorbing medium are solved numerically<sup>25</sup> for a closed two-level system.<sup>26</sup> Although the RP structure can be described analytically for weak absorptions<sup>27</sup> (or in terms of an integral transform<sup>28</sup>), for the present experiments, a numerical approach is necessary to include nonlinear effects arising from high optical densities. We show that the Maxwell Bloch model is in excellent agreement with the experimental measurement. Therefore, using the results of the model, and comparing the calculated signals to those measured experimentally, it is possible to predict the population transfer in

rovibrational transitions and to suggest optimum parameters for optical pumping experiments. The paper concludes with a discussion of the future uses of QCLs for population transfer.

## II. THEORY

### A. Maxwell Bloch equations

The transmission of the QCL radiation through the absorbing gas has been modelled by solving the coupled Maxwell Bloch equations for an inhomogeneously broadened two-level system.<sup>25</sup> A brief outline of the theory and the numerical methods used to solve these equations is given here.

The laser radiation is assumed to be a plane polarised electromagnetic wave travelling along the  $z$ -direction with a linearly increasing angular frequency in time,  $\omega(t)$ , which is close to the molecular transition frequency  $\omega_0$ . To describe the propagation of the radiation, the Maxwell wave equation for a non-magnetic medium with no free charges is used. Assuming that the phase-matching condition  $k = \omega/c$  is met, this equation can be written as

$$\left(\frac{\partial}{\partial z} + \frac{1}{c}\frac{\partial}{\partial t}\right)\tilde{\mathcal{E}}(z, t) = \frac{ik}{2\epsilon_0}\tilde{\mathcal{P}}(z, t), \quad (1)$$

in which  $\tilde{\mathcal{E}}(z, t) = \mathcal{E}(z, t)e^{-i\phi(z, t)}$ , is the complex envelope function describing the amplitude and phase of the electric field under the slowly varying envelope approximation and  $\tilde{\mathcal{P}}(z, t)$  is the macroscopic polarisation density generated by the transition electric dipole moments of the gas molecules. The envelope function for the polarisation density is chosen to be of the form

$$\tilde{\mathcal{P}}(z, t) = \mathcal{N}d(m_J)[\langle u(z, t) \rangle - i\langle v(z, t) \rangle]e^{-i\phi(z, t)}, \quad (2)$$

where  $\mathcal{N}$  is the number density of the absorbing species,  $d$  is the transition dipole moment, and  $\langle u(z, t) \rangle$  and  $\langle v(z, t) \rangle$  are averages over the Doppler profile of the components of the Feynman-Bloch vector (*vide infra*) used to describe the two-level system. The Feynman-Bloch vectors of molecules in different  $m_J$  states, with different transition dipole moments with respect to the laser polarisation,

$$d(m_J) = d\sqrt{\frac{J^2 - m_J^2}{(2J+1)(2J-1)}}, \quad (3)$$

are summed directly with weightings corresponding to their degeneracies. The  $\langle u(z, t) \rangle$  and  $\langle v(z, t) \rangle$  components of the Feynman-Bloch vector determine the absorption and dispersion of the field,<sup>25</sup> while the third component,  $\langle w(z, t) \rangle$ , describes the population inversion in the two-level state and allows the population transfer between the two levels to be calculated. Equation (1) can be rewritten in terms of the real quantities,  $\langle u(z, t) \rangle$  and  $\langle v(z, t) \rangle$ , as

$$\left(\frac{\partial}{\partial z} + \frac{1}{c}\frac{\partial}{\partial t}\right)\Omega = \frac{\mu}{4}\langle v(z, t) \rangle, \quad (4)$$

$$\Omega\left(\frac{\partial}{\partial z} + \frac{1}{c}\frac{\partial}{\partial t}\right)\phi = -\frac{\mu}{4}\langle u(z, t) \rangle, \quad (5)$$

in which the electric field amplitude has been replaced by the Rabi frequency,

$$\Omega(z, t) = \frac{d \times \mathcal{E}(z, t)}{\hbar}, \quad (6)$$

and the constants are represented by one term,

$$\mu = \frac{\mathcal{N}d^2\omega_0}{\epsilon_0\hbar c}. \quad (7)$$

Transforming this pair of equations to the retarded time reference frame by making the substitutions  $T = t - z/c$  and  $Z = z$  gives

$$\frac{\partial \Omega}{\partial Z} = \frac{\mu}{4} \langle v(Z, T) \rangle, \quad (8)$$

$$\Omega \frac{\partial \phi}{\partial Z} = -\frac{\mu}{4} \langle u(Z, T) \rangle. \quad (9)$$

Here, Eq. (9) is used to determine the evolution of the transition dipole moments of the gas molecules, as represented by the Feynman-Bloch vectors, in response to the applied radiation. This evolution is calculated by solving the quantum Liouville equation for the density matrix of a dipole-coupled two-level system. Making use of the rotating-wave approximation, these equations are given in the Feynman-Bloch representation by

$$\dot{u} = -(\Delta - \dot{\phi})v - u/T_2, \quad (10)$$

$$\dot{v} = +(\Delta - \dot{\phi})u + \Omega w - v/T_2, \quad (11)$$

$$\dot{w} = \Omega v - (w - w_{\text{eq}})/T_1, \quad (12)$$

in which,  $u(T)$ ,  $v(T)$ , and  $w(T)$  are the components of Feynman-Bloch vector,  $T_1$  and  $T_2$  are the longitudinal and transverse relaxation times, respectively, and  $w_{\text{eq}}$  is the equilibrium population inversion between the two levels ( $w_{\text{eq}} = -1$  for the calculations here). The longitudinal relaxation time ( $T_1$ ) governs the population decay rate, and the transverse relaxation time ( $T_2$ ) determines the dephasing of the Feynman-Bloch vectors. In the case of constant Rabi frequency and laser detuning, analytical solutions for Eqs. (10)–(12) have been derived by Torrey using the Laplace transform. Details of these solutions are summarised in the Appendix.

## B. Numerical solutions

A spectral method based on Chebyshev grid points was used to solve Eqs. (8) and (9) for the spatial dependence of the QCL radiation (phase and field) along the gas cell of length,  $L$ . Boundary conditions for these equations are determined by  $\phi(Z = 0, T) = 0$ , and by the electric field magnitude,  $\mathcal{E}(Z = 0, t) = \sqrt{2I/\pi\epsilon_0 cr^2}$ , calculated from the power,  $I = 15$  mW, and beam radius,  $r = 1$  mm, of the incident laser radiation. The response of the gas medium to the laser radiation is calculated at each grid point from an ensemble of Feynman-Bloch vectors associated with molecules of different velocities and transition dipole moments. A

TABLE I. Typical parameters used in the Maxwell Bloch simulation. The number of grid points for distance and time depend on the chirp rate used, and the order of the Gauss-Hermite quadrature on the gas pressure. The parameters here were used in Figure 1.

| Simulation parameter                                    | Value               |
|---|---------------------|
| Transition dipole moment (D)                            | 0.0237 <sup>a</sup> |
| Self broadening coefficient (MHz Torr <sup>-1</sup> )   | 5.7                 |
| Laser power (mW)  | 15                  |
| Beam waist radius (mm)                                  | 1                   |
| Path length (m)   | 238, 47 or 1        |
| Order of Gauss-Hermite quadrature (for Doppler average) | 11                  |
| Number of Chebyshev points                              | 11                  |
| Time step (ns)  | 1.8                 |

<sup>a</sup>Calculated from HITRAN (Ref. 29) values, comparable to Ref. 30.

Gauss-Hermite quadrature is used to integrate over the one-dimensional Doppler profile of the gas. The initial conditions for the Feynman-Bloch vectors are the equilibrium values of the Torrey solutions for an electric field  $\mathcal{E}(Z, t = 0) = \mathcal{E}(Z = 0, t)$ , and an initial detuning much larger than the Doppler width of the absorption profile. Each of the Feynman-Bloch vectors are evolved over discrete time steps using the analytical Torrey solutions, assuming implicitly that the frequency of the laser radiation and local Rabi frequency are constant over the time step, valid as  $\Delta t \rightarrow 0$ . The derivative  $\dot{\phi}(Z, T)$  appearing in Eqs. (10) and (11) is calculated using a second-order finite difference. The transmittance of the gas as a function of time is calculated from the electric field magnitude at the detector,  $T(t) = [\mathcal{E}(L, t)/\mathcal{E}(0, t)]^2$ . To compare with the experimental signal, the calculated transmittance is convoluted with a Gaussian function with a full width at half maximum corresponding to the acquisition system time response.

## C. Calculated examples

In order to test the model, average values for the three Feynman-Bloch vector components,  $\langle v \rangle$ ,  $\langle u \rangle$ , and  $\langle w \rangle$ , are calculated by integrating over the path length,  $m_J$  states and velocity distribution of the molecules. Table I summarises the parameters used, and Figure 1 displays the results.

The relaxation times  $T_1$  and  $T_2$  are assumed to be equal at a given gas pressure<sup>27</sup> and are calculated from the self-broadening coefficient of the  $2\nu_2$  P(42) transition of OCS from  $T_1 = T_2 = 1/(p\gamma_{\text{self}})$ , where  $p$  is the pressure of OCS, and  $\gamma_{\text{self}}$  the self-broadening coefficient obtained from HITRAN.<sup>29</sup> The relaxation time determines the temporal decay of the signal, as shown in Figure 1(a). The oscillations depend upon the chirp rate, as this will affect the rate of change of the detuning through the resonance. Therefore, a relatively high chirp rate of 100 MHz ns<sup>-1</sup> was used, so that clear oscillations are shown in this example. These oscillations arise when the detuning away from resonance causes a rotation in the Feynman-Bloch vector, which precesses back to the ground state, as shown in Figure 1(b).

When the relaxation time is much longer ( $T_1 = T_2 = 27.8$   $\mu\text{s}$ ) than the time taken for the laser to sweep through the transition (0.5 ns), there is minimal relaxation during the chirp, so that large oscillations are

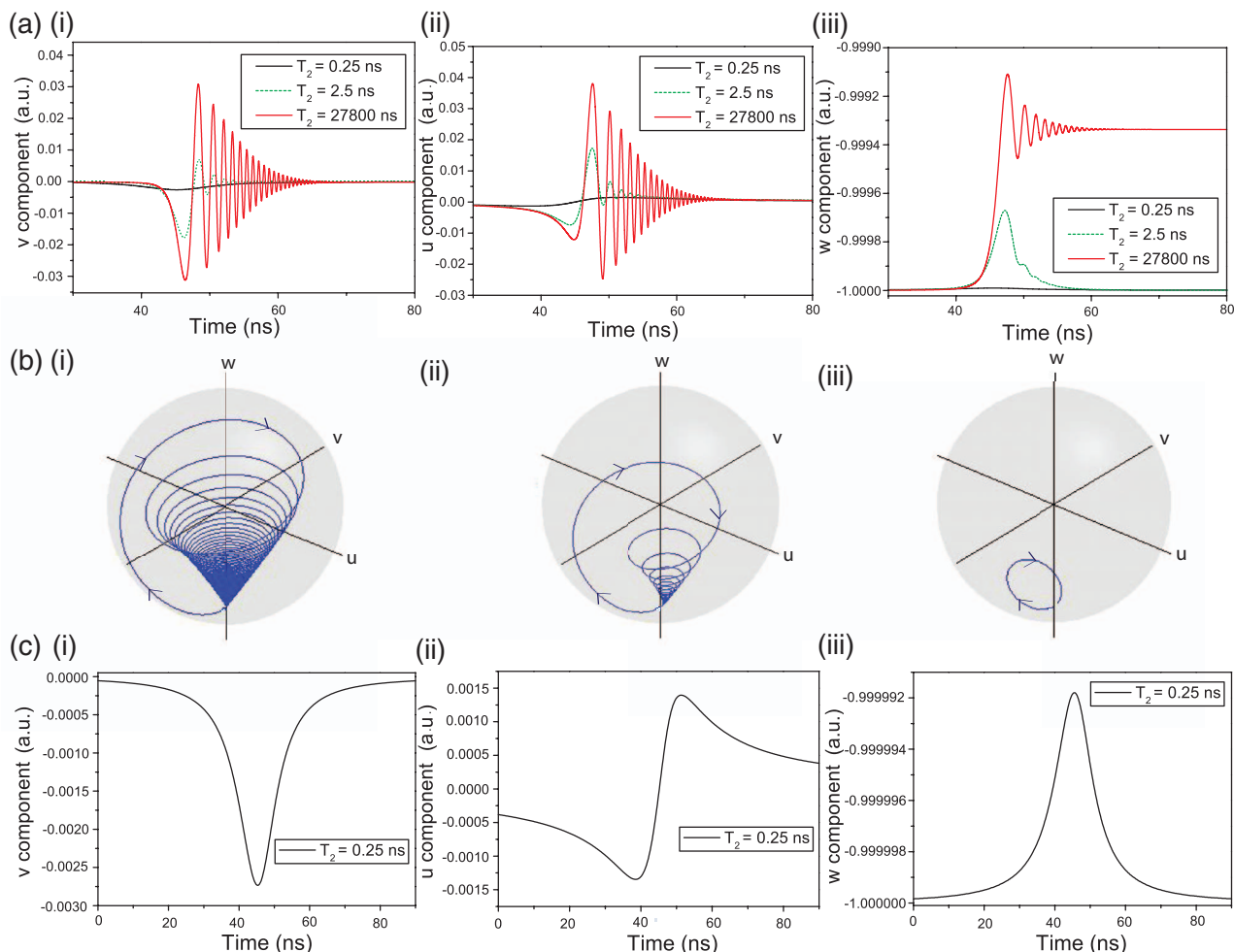


FIG. 1. (a) Example solutions to the Maxwell Bloch equations for different relaxation times. The calculations were performed using a chirp rate of  $100 \text{ MHz ns}^{-1}$ , a path length of  $1 \text{ m}$  and other parameters as given in Table I. (i–iii) The average values of the  $\langle v \rangle$ ,  $\langle u \rangle$ , and  $\langle w \rangle$  Feynman-Bloch vector components over the path length as a function of time. (b) Solutions plotted on the Bloch sphere, using the same parameters as in (a), but, for clarity, the Rabi frequency has been increased by a factor of  $10^3$  and relaxation times,  $T_2$  of (i)  $5 \text{ ns}$  (ii)  $1.5 \text{ ns}$ , and (iii)  $0.1 \text{ ns}$ . (c) For relaxation times which are much shorter than the time taken for the laser frequency to sweep through the transition, an equilibrium absorption profile is recovered, as reflected in the  $\langle v \rangle$  component shown in (i). The  $\langle u \rangle$  component is in this case given by the Kramers-Kronig relation, giving a dispersion profile as shown in (ii), while the  $\langle w \rangle$  component follows the absorption profile, as shown in (iii).

observed in the  $\langle v \rangle$ ,  $\langle u \rangle$ , and  $\langle w \rangle$  components in Figure 1(a). By decreasing the  $T_1 = T_2$  values, relaxation occurs faster, so that fewer oscillations are observed, and when the relaxation time is comparable to the time for the laser to sweep through the resonance, the  $\langle v \rangle$  and  $\langle u \rangle$  components look, respectively, like an equilibrium absorption profile (see Figure 2), and a dispersion profile from the Kramers-Kronig relations, shown in Figure 1(c). The predicted population transfer in the two-level system can be calculated from  $(\langle w \rangle + 1)/2$ , and it is averaged over the path length,  $m_J$  states and velocity components. Therefore, once the model reproduces quantitatively the absorption signals under a RP regime, it will also give a quantitative estimate of the population transfer achieved. We have further checked our simulations by comparison to Ref. 21. In addition, the population transfer between the  $v = 1 \leftarrow 0$  states of NO as in Ref. 7 was calculated by solving the Maxwell Bloch equations for this system, and the result is comparable to the experimentally detected population in the  $v = 1$  state. Considering the experimentally

observed transmission signals from a selection of different experiments can be modelled, this gives confidence that the correct degree of population transfer can be predicted.

### III. EXPERIMENTAL

The  $9.7 \mu\text{m}$  distributed feedback cw-QCL (Hamamatsu, L10195-9700) can be operated in the range of  $1027.78 \text{ cm}^{-1}$ – $1034.22 \text{ cm}^{-1}$ . The laser is sealed in a temperature controlled mount (ILX Lightwave LDM-4872) and cooled to  $-4 \text{ }^\circ\text{C}$  to access the  $2\nu_2$  P(42) transition of OCS, and stabilised using a temperature controller (ILX Lightwave LDT-5545B). A high compliance laser diode current source (ILX Lightwave LDX-3232) was used to set the dc current through the QCL and the laser emission frequency was tuned by varying this current in combination with the temperature of the laser chip. The laser emission frequency was scanned, typically by around  $0.1 \text{ cm}^{-1}$ , using a function generator (Tectronix AFG-3022B) to apply a dc current ramp over the set current level. The

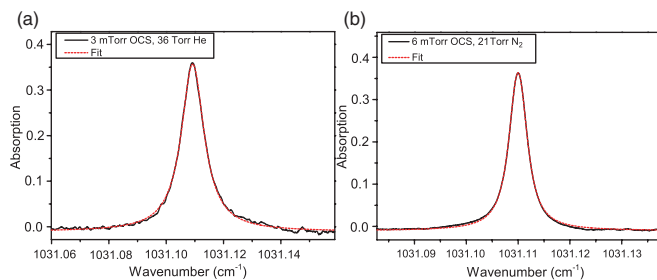


FIG. 2. The buffered spectra for low pressures of OCS in the Herriott cell, in order to verify the two path lengths used as (a) 238 m, and (b) 47 m for the  $2\nu_2$  P(42) transition of OCS, located at  $1031.109\text{ cm}^{-1}$ .

laser output was collimated using a 4.8 mm focal length anti-reflection coated lens (Hamamatsu, A11331-01) to produce a beam of radius  $\sim 1$  mm. The beam was reflected by three mirrors and passed into an astigmatic Herriott cell (Aerodyne Research Inc) with a 1 m base length, and a maximum 238 m path length. From the exit of the Herriott cell, the beam was directed by two mirrors onto a 1 GHz, ac-coupled detector (VIGO System 3PVI-3TE-10.6). The signal from the detector was recorded using a 200 MHz, 2 gigasample/s oscilloscope (LeCroy Wavesurfer 424).

For the present study, two different path lengths were obtained by adjusting the incidence angle of the cw-QCL beam on entry into the Herriott cell. Conventional absorption spectroscopy was used to verify the path length in both cases: approximately 30 Torr of  $\text{N}_2$  or He was added as a buffer gas to a low pressure of OCS (mTorr), allowing a symmetric absorption line shape to be observed, as shown in Figure 2. Voigt fits of the spectra confirmed the expected path length of 238 m, and 47 m, respectively, for the  $2\nu_2$  P(42) transition of OCS, located at  $1031.109\text{ cm}^{-1}$ , with an integrated absorption cross section of  $2.581 \times 10^{-21}\text{ cm}^{-1}$  ( $\text{molecule}^{-1}\text{cm}^{-2}$ ).<sup>29</sup> Pressure broadening coefficients obtained from Voigt fits using a constrained Doppler width were in good agreement with those in the HITRAN database.<sup>29</sup>

The current ramp applied to the laser modulates both the power and wavelength of the emitted radiation. A typical variation in intensity over a modulation cycle is shown in Figure 3(a) in which the positive gradient and negative gradient correspond to a down- and up-chirp, respectively. It should be noted that the time at which the frequency chirp changes from down- to up-chirp does not coincide with the times at which the laser intensity signal is at a maximum or minimum, (see Figure 3(a)), but is displaced temporally as a result of the response of the laser control electronics. The position of this change-over time, determined by observing the transitions when changing the applied current to the laser, is marked on Figure 3(b).

Calibration of the laser frequency and chirp rate was achieved by passing the laser radiation through a 3-in. long germanium etalon with a free spectral range of 480 MHz. A typical transmission signal through the etalon is shown in Figure 3(b). Changing the current slope from  $0.002\text{ mA ns}^{-1}$  to  $0.02\text{ mA ns}^{-1}$  allows almost an order of magnitude difference in chirp rate to be accessed, as shown in Table II. The

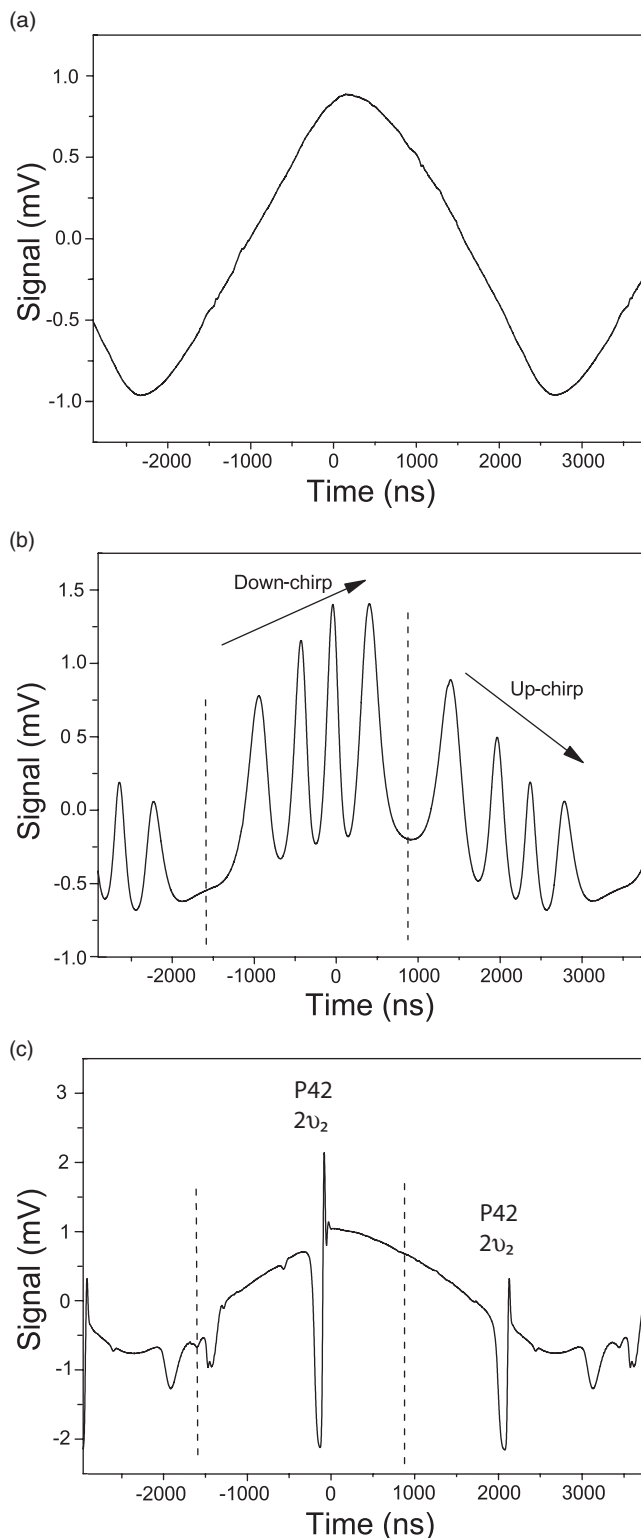


FIG. 3. (a) Spectrum showing the variation in intensity of the laser radiation due to the voltage ramp, (b) spectrum showing the laser transmission through the 480 MHz germanium etalon; the down-chirp, up-chirp and “change over” (dotted line) points are marked, (c) shows a sample OCS spectrum during the down- and the up-chirp phases of the scan. There are small oscillations in the baseline in (a) at the “change over” point due to the laser control electronics. Note that the position of the RP signal is always later in time compared to the absorption.

TABLE II. The change in chirp rate on application of the voltage ramp to the laser chip at various frequencies.

| Current slope<br>(mA ns <sup>-1</sup> ) | Calculated chirp rate<br>(MHz ns <sup>-1</sup> ) | Calculated resolution<br>(MHz) |
|---|--|--------------------------------|
| 0.02                                    | 1.08   | 30.9                           |
| 0.01                                    | 0.76   | 25.9                           |
| 0.005                                   | 0.42   | 19.3                           |
| 0.002                                   | 0.13   | 10.7                           |

spectral resolution is calculated from

$$\Delta\nu = \sqrt{C \frac{d\nu}{dt}}, \quad (13)$$

where  $d\nu/dt$  is the calculated chirp rate of the cw-QCL, and  $C$  is a constant that depends on the characteristics of the acquisition system (here assumed to be 0.886 (Ref. 31)). For a symmetric ramp, the chirp rate was calculated at the centre of each down- and up-chirp, and was found to be the same for each. Although a small variation in the chirp rate was observed at the ends of the voltage ramp, tuning the offset current applied to the laser ensured that the molecular absorptions occurred during the central part of the ramp. By applying a sawtooth voltage ramp, different chirp rates are produced on the rising and falling edges of the modulation, allowing the effects of chirp rate in the observed spectra to be explored concurrently. An example of the signals observed using a low pressure of OCS is shown in Figure 3(c). It can be seen that the RP features occur later in time than the main absorption feature, i.e., post-resonance and irrespective of the direction of the frequency chirp. This behaviour is expected, as in order to observe this type of interference effect, the laser radiation must first produce a polarised sample. Although no dependence on the direction of the frequency chirp has been observed, for consistency, unless otherwise stated, we consider only the molecular absorptions recorded using the down-chirp, such that the RP features appear on the lower frequency side of the transition. An important point to note is that at the very low chirp rates used, the chirp-limited resolution, calculated from Eq. (13) and shown in Table II, reaches sub-Doppler levels (the Doppler width is 49.5 MHz).

## IV. RESULTS

### A. Chirp rate variation

As noted in the Introduction, the laser chirp rate is of central importance for experiments using rapidly swept radiation sources. Applying an asymmetric ramp to the cw-QCL, allowed two different chirp rates to be accessed within one modulation cycle. Raw signals associated with the molecular transitions, recorded using chirp rates of 1.5 MHz ns<sup>-1</sup> – 0.8 MHz ns<sup>-1</sup>, are shown in Figure 4(a). Corresponding transmission signals, in which the laser power variation over the modulation cycle has been removed, are shown in Figure 4(b). For the highest chirp rate of 1.5 MHz ns<sup>-1</sup> it takes  $\sim 0.03\mu\text{s}$  for the laser frequency to pass through the Doppler width of the OCS transition. This is much less than the

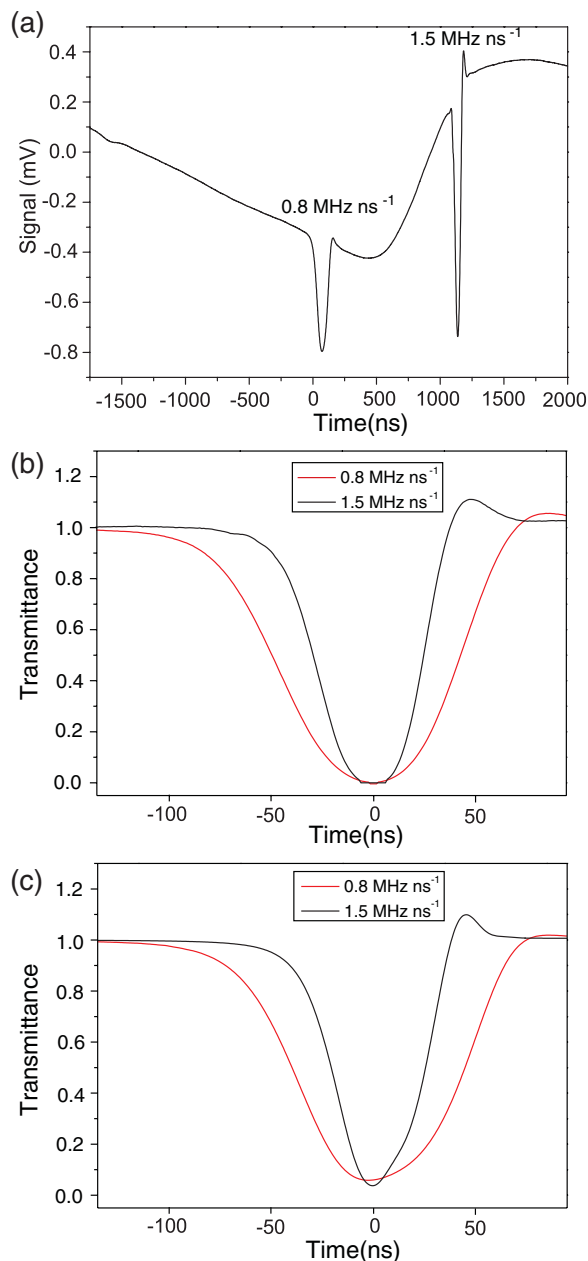


FIG. 4. (a) Experimental spectrum of 7 mTorr OCS in the Herriot cell with a 238 m path length displaying an asymmetric laser chirp so that the up-chirp (down-chirp) has a chirp rate of 0.8 MHz ns<sup>-1</sup> (1.5 MHz ns<sup>-1</sup>). The observed P(42) OCS spectra as a function of time for (b) experiment, (c) theory.

pressure-limited relaxation time of  $T_1 = T_2 = 4\mu\text{s}$  expected for this transition using 7 mTorr of OCS. Consequently, for the chirp rates used, the relaxation of the induced polarisation in the sample is slow in comparison to the time required to sweep through the Doppler width of the transition, leading to RP effects in the experimental signals. These features are captured well by the absorption signals calculated using the approach detailed in Sec. II A and shown in Figure 4(c). As the chirp rate is decreased, both the experimental and theoretical absorption signals are observed to become broader and the RP oscillation more damped.

It should be noted that once the time axes of the spectra are converted to wavenumbers using the etalon calibra-

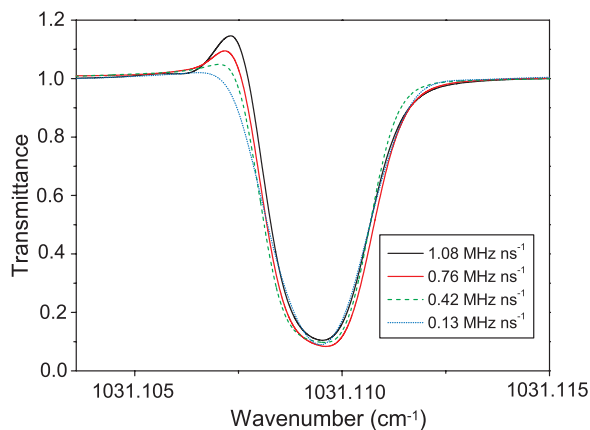


FIG. 5. Experimental spectra showing the effect of different chirp rates on the RP signals for the P(42) transition measured using 4 mTorr of OCS and a path length of 238 m.

tion, the widths of the transitions are similar at all chirp rates, as seen in Figure 5 for chirp rates in the range of 0.13–1.08 MHz ns<sup>-1</sup>. As in the previous example, the transmission intensity of the post-resonance rapid passage signal decreases as the chirp rate is decreased. This behaviour arises because, at low chirp rates, the time needed for the laser radiation to become in-phase with the induced polarisation is increased. This allows the polarisation to decay before appreciable constructive interference can occur and so both the intensity and the frequency of the RP oscillations are reduced.

For very low chirp rates, the laser radiation remains close to resonance for an extended period and this allows more pronounced rotation of the Feynman-Bloch vector in the direction of higher population inversion. This is illustrated in Figure 6(a), which shows the simulated  $\langle w \rangle$ -components for this range of chirp rates and at an OCS pressure of 4 mTorr, plotted together with the predicted population transfer to the  $2\nu_2$  P(42) OCS state. As the chirp rate decreases from 100 to 5 MHz ns<sup>-1</sup>, the calculated population transfer increases. In Figure 6(b) the calculated maximum population transfer from the  $\langle w \rangle$ -parameter output from the Maxwell Bloch simulation is plotted for a range of chirp rates. In this system  $\Omega_0$

= 3 MHz and so the adiabatic condition of  $\Omega_0^2 \gg d\omega(t)/dt$  is not satisfied until the chirp rate approaches 0.1 MHz ns<sup>-1</sup>. As a result, a sharp increase in the predicted population transfer is observed for chirp rates around this value. This demonstrates the importance of achieving a suitably low chirp rate in order for population transfer to occur efficiently.

## B. Optically thick samples

A further test of the Maxwell Bloch model is to compare the transmission signals simulated for optically thick samples where the absorbance,  $A = \sigma(\frac{N}{L})l \gg 1$ . Previous similar experiments in this regime using a pulsed QCL system,<sup>26,32,33</sup> found a broadening of the absorption signal that was several orders of magnitude greater than would be expected for pressure-induced broadening of a transition under linear conditions (in the absence of RP effects). This broadening results in a shift to later times during the pulse of the “peak” associated with the rapid passage signal. This shift can be calculated by comparing the position of the RP maximum peak and the wavenumber of the transition taken from HITRAN.<sup>29</sup> In the previous studies with pulsed QCLs, it was found that the shift was independent of the intensity of the laser radiation and chirp rate,<sup>32</sup> while shorter path lengths resulted in smaller shifts. In the present work, the shift in RP signals with increasing pressure of OCS is studied using a cw-QCL with a much lower chirp rate and using larger path lengths. The increased path length allows a high optical thickness to be maintained while using relatively low pressures of OCS, thereby ensuring that the sample, while being optically thick, is minimally damped by collisional relaxation.

The effect of increasing the optical thickness on the absorption spectrum was investigated by comparing the experimental and simulated signals of increasing pressures of OCS in the Herriott cell. The range of OCS pressures used were between 1 mTorr and 130 mTorr, at path lengths of 47 m and 238 m. The chirp rate was kept at the same value for all measurements at each path length (1 MHz ns<sup>-1</sup> at 238 m and 3 MHz ns<sup>-1</sup> at 47 m; but this small change does not affect the shift<sup>33</sup>), allowing the results to be compared.

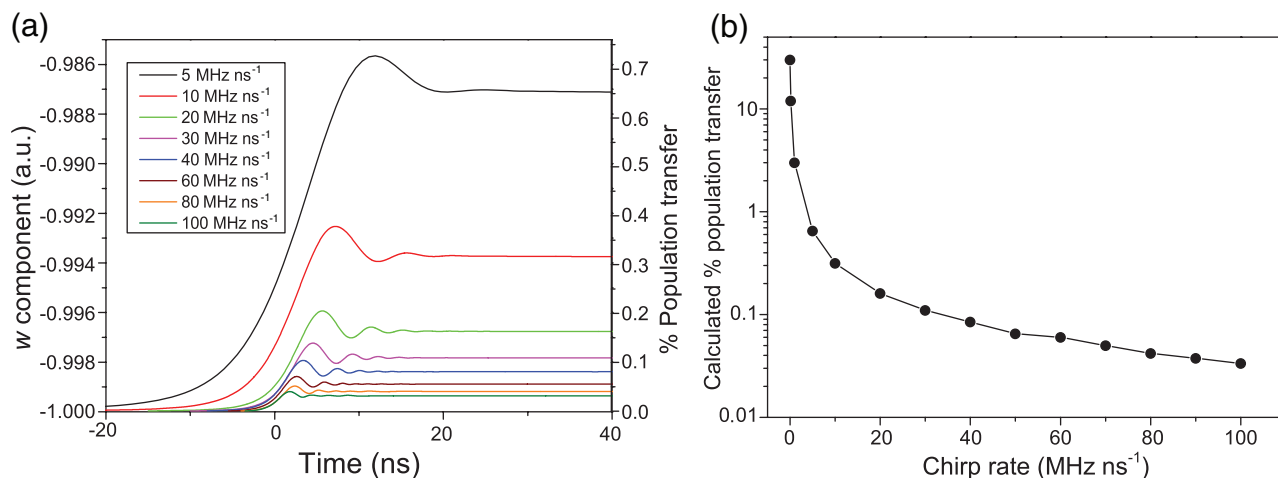


FIG. 6. (a) Population transfer for the  $2\nu_2$  P(42) transition of OCS as a function of the chirp rate of the cw-QCL, calculated for a path length of 238 m and an OCS pressure of 4 mTorr, (b) log plot showing the population transferred after the cw-QCL pulse as a function of chirp rate.

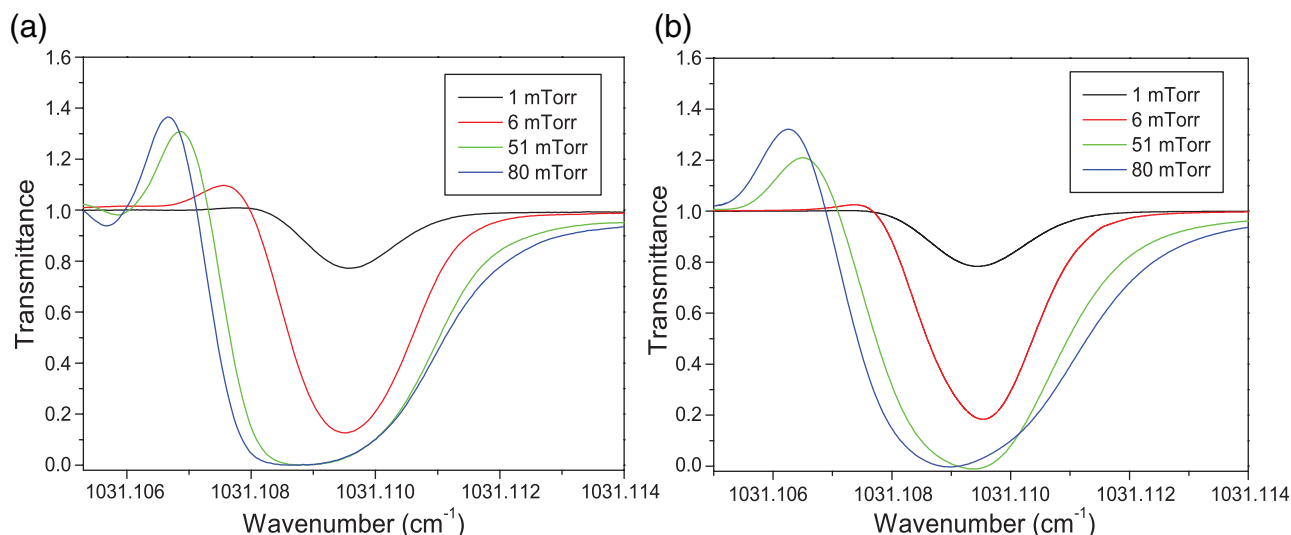


FIG. 7. Data showing the change in absorption spectra of the OCS transition as a function of pressure at a chirp rate of  $3 \text{ MHz ns}^{-1}$  and a path length of 47 m for (a) experiment, (b) theory.

Figure 7(a) displays representative spectra for increasing pressures of OCS and, again, the absorption profiles increase in width and there is a shift in time (and therefore wavenumber) where the rapid passage peak occurs (relative to the low pressure spectra). In Figure 7(b) it can be seen that the simulation correctly models how the RP signals evolve as the pressure of OCS increases. It has been noted previously in experimental pulsed-QCL studies that the RP shift measured for increasing gas pressures is dependent on the dipole moment of the molecule<sup>34</sup> and the optical path length of the propagation of the beam.<sup>33</sup> The shift is affected minimally by the incident laser power and chirp rate.<sup>34</sup> Considering that the OCS shift recorded with a cw-QCL is well modelled by the two-level Maxwell Bloch model, as displayed in Figure 8 for two different path lengths, it is evident that the shift occurs solely due to the increased optical density in the cell as the gas pressure is increased.

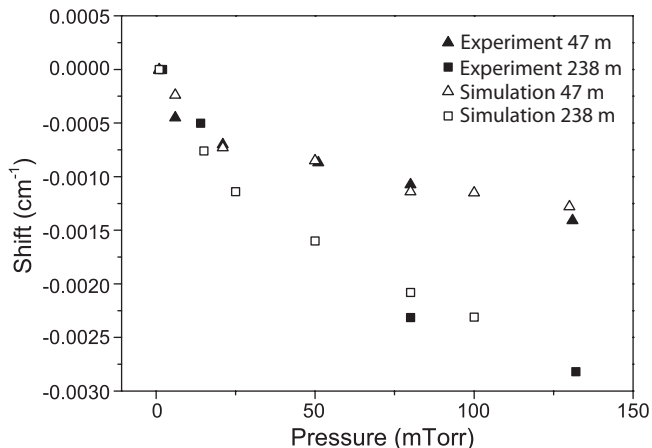


FIG. 8. Pressure shifts for the P(42) OCS transition at the chirp rates shown for two absorption path lengths of 47 m and 238 m. Both the experimentally (filled symbols), and the simulated (open symbols) shifts are shown.

## V. DISCUSSION AND CONCLUSION

A modulated cw-QCL was used to observe absorption spectra of OCS in a 238 m Herriott cell, in which all display the effects of rapid passage. The experimental signals for a variety of chirp rates, gas pressures, and path lengths are well-simulated by the Maxwell Bloch equations for an inhomogeneously broadened two-level system. That the observed signals can be described by the Maxwell Bloch equations alone, suggests that other factors thought to affect the RP signals, e.g., the effects of self-focusing,<sup>26</sup> are negligible. The population transfer in the current experiments have been inferred from the simulations, which themselves agree well with recent measurements using two cw-QCLs in a pump-probe arrangement.<sup>7</sup>

The predicted population transfer to the  $2\nu_2$  P(42) state of OCS is seen to depend strongly on the chirp rate of the laser, and to a lesser extent on the pressure of the OCS gas; little difference was observed after changing the path length, even for optically thick samples. At the lowest chirp rate of  $0.13 \text{ MHz ns}^{-1}$ , the population transfer is calculated to be 12%, considerably more than the 0.03% calculated for a chirp rate of  $100 \text{ MHz ns}^{-1}$  typical for a pulsed QCL. This shows that the lower the chirp rate in this system, the more effectively population can be transferred to the upper state. However, it should be noted that there will be an optimum minimum chirp rate as, for very low chirp rates, relaxation effects will return the system to an equilibrium population distribution.

Factors affecting the population transfer that can be achieved between rovibrational states in the infrared region by using cw-QCLs have been discussed using the predictions of the Maxwell Bloch model. In order to achieve efficient population transfer, the relaxation of the system needs to be slow in comparison to the time taken to sweep through the Doppler width of the transition. Increasing the Rabi frequency also improves the efficiency: in the Feynman-Bloch model of the optical excitation, the vector rotates more quickly, reaching

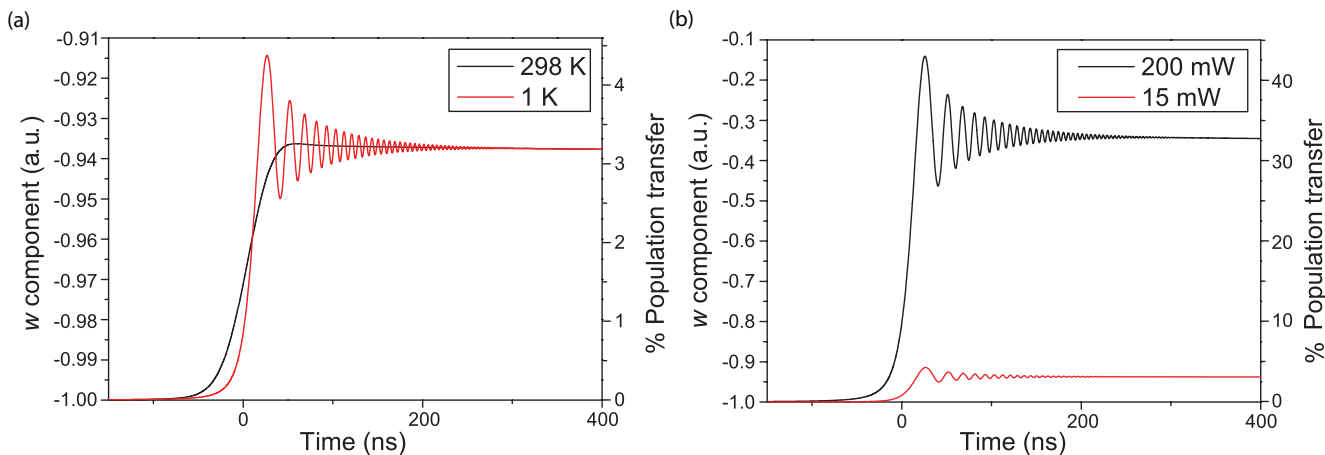


FIG. 9. Calculated  $\langle w \rangle$  components and population transfers for the  $2\nu_2$  P(42) OCS transition, a number density of  $10^{13}$   $\text{cm}^{-3}$ , chirp rate of  $1$   $\text{MHz ns}^{-1}$  and an incident laser power of  $15$   $\text{mW}$ , at (a) temperatures of  $1$   $\text{K}$  and  $298$   $\text{K}$ . (b) Same parameters but for a temperature of  $1$   $\text{K}$ , and a higher incident power of  $200$   $\text{mW}$ .

a higher population transfer within the duration of the laser pulse.

The degree of population transfer can be increased, for example, if a pulsed molecular beam is used instead of the room-temperature cell here. The effect of modifying the temperature on the  $\langle w \rangle$ -component output from the Maxwell Bloch simulation is shown in Figure 9(a) for the P(42) transition of OCS at a chirp rate of  $1$   $\text{MHz ns}^{-1}$ , and a number density of  $10^{13}$   $\text{cm}^{-3}$  (typical for a pulsed beam). The temperature is varied from  $298$   $\text{K}$  to  $1$   $\text{K}$ , a temperature that may be achieved using a skimmed molecular beam. It can be seen that the effect of the change in temperature is to increase the coherence in the prepared state. Therefore, utilising the low chirp rates of a cw-QCL and the typical low temperature in a molecular beam may be a way to achieve significant coherent state preparation, in order to study vibrationally excited species. Using a higher power cw-QCL ( $200$   $\text{mW}$ , which is commercially available), increases the Rabi frequency and, in this case, a higher population transfer is predicted, as seen in Figure 9(b). It should also be noted that this work employs an overtone transition, and a significantly higher population transfer would be achievable by using a fundamental transition in a small polyatomic molecule such as  $\text{O}_3$  or  $\text{NH}_3$ . Future experiments in this area may also include the development of QCL-based infrared stimulated Raman adiabatic passage.<sup>35</sup>

## ACKNOWLEDGMENTS

This work is conducted under the EPSRC programme grant EP/G00224X/1: New Horizons in Chemical and Photochemical Dynamics.

## APPENDIX: ANALYTICAL SOLUTIONS TO THE MAXWELL BLOCH EQUATIONS

In order to make explicit our use of the analytic solutions to the Maxwell Bloch equations, a summary of the results obtained by Torrey<sup>36</sup> is given here. Using the same notation as Bloch,<sup>14</sup> the differential equations governing the evolution of the components of the Feynman-Bloch vector can be written as

$$du/d\tau + \beta u + \delta v = 0, \quad (\text{A1})$$

$$dv/d\tau + \beta v - \delta u + M_z = 0, \quad (\text{A2})$$

$$dM_z/d\tau + \alpha M_z - v = \alpha M_0, \quad (\text{A3})$$

where, for the case of an optically driven two-level system with longitudinal and transverse relaxation times  $T_1$  and  $T_2$ , respectively, and with an equilibrium population

TABLE III. Analytic expressions for the coefficients of the transient and steady-state terms in Eq. (A4).

|        | $u/M_0$  | $v/M_0$   | $M_z/M_0$   |
|--------|--|---|---|
| $g(p)$ | $u_0 p [1 + (p + \alpha)(p + \beta)] + \delta(\alpha + m_0 p) - \delta v_0 p (p + \alpha)$ | $u_0 \delta p (p + \alpha) + v_0 p (p + \alpha)(p + \beta) - (\alpha + m_0 p)(p + \beta)$ | $u_0 \delta p + v_0 p (p + \beta) + (\alpha + m_0 p)[(p + \beta)^2 + \delta^2]$ |
| A      | $-g(-a)/a[(b-a)^2 + s^2]$  | $-g(-a)/a[(b-a)^2 + s^2]$   | $-g(-a)/a[(b-a)^2 + s^2]$   |
| B      | $-(A + D) + u_0$   | $-(A + D) + v_0$  | $-(A + D) + m_0$  |
| C      | $aA + bB - \beta u_0 - \delta v_0$   | $aA + bB - m_0 + \delta u_0 - \beta v_0$  | $aA + bB + \alpha(1 - m_0) + v_0$   |
| D      | $\alpha \delta / [\alpha(\beta^2 + \delta^2) + \beta]$                                     | $-\alpha \beta / [\alpha(\beta^2 + \delta^2) + \beta]$                                    | $\alpha(\beta^2 + \delta^2) / [\alpha(\beta^2 + \delta^2) + \beta]$             |

inversion of  $w_{\text{eq}}$ ,

$$\begin{aligned}\tau &= \Omega t, & \delta &= (\omega_0 - \omega)/\Omega, \\ \alpha &= 1/\Omega T_1, & \beta &= 1/\Omega T_2, \\ M_z &= -w, & M_0 &= -w_{\text{eq}}.\end{aligned}$$

These equations can be solved using the Laplace transform to give a general solution of the form,

$$y(t) = Ae^{-at} + Be^{-bt} \cos st + \frac{C}{s} e^{-bt} \sin st + D, \quad (\text{A4})$$

in which  $y$  stands for any one of the components  $u/M_0$ ,  $v/M_0$  or  $w/M_0$ . The parameters appearing in Eq. (A4) can be calculated as follows. The most negative real root of the polynomial equation,

$$\Delta(p) = (p + \alpha)(p + \beta)^2 + p + \beta + \delta^2(p + \alpha) = 0, \quad (\text{A5})$$

is equal to  $-a$ , which allows the two other constants governing the transient behaviour of the solution to be computed straightforwardly,

$$b = (\alpha + 2\beta - a)/2, \quad (\text{A6})$$

and

$$s = \sqrt{1 + 2\beta\alpha + \beta^2 + \delta^2 - 2ab - b^2}. \quad (\text{A7})$$

The remaining parameters are determined by the initial conditions, which are written in the form  $u_0 M_0$ ,  $v_0 M_0$ , and  $m_0 M_0$  for each of the components  $u$ ,  $v$ , and  $w$ , respectively. Table III provides a recipe for these calculations.

<sup>1</sup>R. F. Curl, F. Capasso, C. Gmachl, A. A. Kosterev, B. McManus, R. Lewicki, M. Pusharsky, G. Wysocki, and F. K. Tittel, *Chem. Phys. Lett.* **487**, 1 (2010).

<sup>2</sup>J. Faist, F. Capasso, D. L. Sivco, C. Sirtori, A. L. Hutchinson, and A. Y. Cho, *Science* **264**, 553 (1994).

<sup>3</sup>F. Capasso, *Opt. Eng.* **49**, 111102 (2010).

<sup>4</sup>J. T. Remillard, D. Uy, W. H. Weber, F. Capasso, C. Gmachl, A. L. Hutchinson, D. L. Sivco, J. N. Baillargeon, and A. Y. Cho, *Opt. Express* **7**, 243 (2000).

<sup>5</sup>G. Duxbury, J. Kelly, T. Blake, and N. Langford, *J. Chem. Phys.* **136**, 174317 (2012).

<sup>6</sup>G. Duxbury, J. Kelly, T. Blake, and N. Langford, *J. Chem. Phys.* **136**, 174319 (2012).

<sup>7</sup>R. J. Walker, J. H. van Helden, J. Kirkbride, E. A. McCormack, M. T. Bell, D. Weidmann, and G. A. D. Ritchie, *Opt. Lett.* **36**, 4725 (2011).

<sup>8</sup>G. Hancock, G. A. D. Ritchie, J. H. van Helden, R. J. Walker, and D. Weidmann, *Opt. Eng.* **49**, 111121 (2010).

<sup>9</sup>R. N. Zare, *Science* **279**, 1875 (1998).

<sup>10</sup>S. Chelkowski, A. D. Bandrauk, and P. B. Corkum, *Phys. Rev. Lett.* **65**, 2355 (1990).

<sup>11</sup>D. J. Maas, D. I. Duncan, A. F. G. van der Meer, W. J. van der Zande, and L. D. Noordam, *Chem. Phys. Lett.* **270**, 45 (1997).

<sup>12</sup>H. Maeda, D. V. L. Norum and T. F. Gallagher, *Science* **307**, 1757 (2005).

<sup>13</sup>A. Bandrauk, *Molecules in Laser Fields* (Marcel Dekker, New York, 1994).

<sup>14</sup>F. Bloch, *Phys. Rev.* **70**, 460 (1946).

<sup>15</sup>N. V. Vitanov, T. Halfmann, B. W. Shore, and K. Bergmann, *Annu. Rev. Phys. Chem.* **52**, 763 (2001).

<sup>16</sup>D. Grischkowsky, *Phys. Rev. A* **14**, 802 (1976).

<sup>17</sup>M. M. T. Loy, *Phys. Rev. Lett.* **32**, 814 (1974).

<sup>18</sup>S. Avriillier, J.-M. Raimond, C. J. Borde, D. Bassi, and G. Scoles, *Opt. Commun.* **39**, 311 (1981).

<sup>19</sup>A. Adam, T. Gough, N. Isenor, and G. Scoles, *Phys. Rev. A* **32**, 1451 (1985).

<sup>20</sup>J. S. Melinger, S. R. Gandi, A. Hariharan, J. X. Tull, and W. S. Warren, *Phys. Rev. Lett.* **68**, 2000 (1992).

<sup>21</sup>G. Duxbury, N. Langford, M. T. McCulloch, and S. Wright, *Chem. Soc. Rev.* **34**, 921 (2005).

<sup>22</sup>T. Beyer, M. Braun, and A. Lambrecht, *J. Appl. Phys.* **93**, 3158 (2003).

<sup>23</sup>M. T. McCulloch, G. Duxbury, and N. Langford, *Mol. Phys.* **104**, 2767 (2006).

<sup>24</sup>G. Duxbury, N. Langford, M. T. McCulloch, and S. Wright, *Mol. Phys.* **105**, 741 (2007).

<sup>25</sup>L. Allen and J. H. Eberly, *Optical Resonance and Two Level Atoms* (Dover, 1975).

<sup>26</sup>G. Duxbury, N. Langford, and K. Hay, *J. Mod. Opt.* **55**, 3293 (2008).

<sup>27</sup>J. C. McGurk, T. G. Schmalz, and W. H. Flygare, *J. Chem. Phys.* **60**, 4181 (1974).

<sup>28</sup>V. V. Khodos, D. A. Ryndyk, and V. L. Vaks, *Eur. Phys. J.: Appl. Phys.* **25**, 203 (2004).

<sup>29</sup>L. S. Rothman, I. E. Gordon, A. Barbe, D. C. Benner, P. F. Bernath, M. Birk, V. Boudon, L. R. Brown, A. Campargue, and J.-P. Champion, *J. Quant. Spectrosc. Radiat. Transf.* **110**, 533 (2009).

<sup>30</sup>K. Tanaka, T. Tanaka, and I. Suzuki, *J. Chem. Phys.* **82**, 2835 (1985).

<sup>31</sup>A. E. Siegman, *Lasers* (University Science Books, 1986).

<sup>32</sup>J. H. van Helden, R. Peverall, G. A. D. Ritchie, and R. J. Walker, *Appl. Phys. Lett.* **94**, 051116 (2009).

<sup>33</sup>J. H. Northern, G. A. D. Ritchie, E. P. Smakman, J. H. van Helden, R. J. Walker, and G. Duxbury, *Appl. Phys. B.* **102**, 37 (2011).

<sup>34</sup>J. H. Northern, G. A. D. Ritchie, E. P. Smakman, J. H. van Helden, J. Cockburn, and G. Duxbury, *Opt. Lett.* **35**, 2750 (2010).

<sup>35</sup>N. Mukherjee and R. N. Zare, *J. Chem. Phys.* **132**, 154302 (2010).

<sup>36</sup>H. Torrey, *Phys. Rev.* **76**, 1059 (1949).